Ceramics-Silikáty 66 (1), 78-84 (2022)
www.ceramics-silikaty.cz 10.13168/cs.2022.0002

Eu-DOPED $La_{1-x}Y_xAlO_3$: IMPACT OF Y/La RATIO ON OPTICAL PROPERTIES

JAN HAVLÍČEK*,#, KATEŘINA RUBEŠOVÁ*, VÍT JAKEŠ*, JAKUB CAJZL*, FILIP PRŮŠA**, ROMANA KUČERKOVÁ***, MARTIN NIKL***

*Department of Inorganic Chemistry, University of Chemistry and Technology, Technická 5, Prague 6, 166 28, Czech Republic
**Department of Metals and Corrosion Engineering, University of Chemistry and Technology, Technická 5, Prague 6, 166 28, Czech Republic
***Institute of Physics of the Czech Academy of Sciences, Cukrovarnická 10, 16200 Prague, Czech Republic

#E-mail: havlicej@vscht.cz

Submitted December 10, 2021; accepted January 12, 2022

Keywords: Perovskite, Ceramics, Optical materials, Luminescence, Spark plasma sintering

$YAlO_3$ and $LaAlO_3$ are both important oxides used as matrices in optical applications. Their mutual solid solubility is kinetically dependent, especially in a polycrystalline form. In this work, we prepared $La_{1-x}Y_xAlO_3$ ($x = 0 – 0.65$) samples doped with 5 at. % of Eu^{3+} in the A-site. The samples were prepared by Spark Plasma Sintering from powders synthetised by a reverse co-precipitation method. The single-phase samples were obtained up to a composition of $La_{0.7}Y_{0.25}Eu_{0.05}AlO_3$; with a higher yttrium doping level, a mixture of Y-rich and La-rich perovskite-type phases was present. The La/Y substitution had an influence on a shift in the top of the valence band which influenced the excitation spectra. In photoluminescence and radioluminescence measurements, the Eu^{3+} local site symmetry changes were manifested by the change in intensity and fine splitting of the $^5D_0 \rightarrow {}^7F_J$ ($J = 1, 2, 3, 4, 5$) emission bands. The increasing content of Y^{3+} caused a slight acceleration of the PL decay of the Eu^{3+} photoluminescence and an increase in the integral intensity of radioluminescence spectra.

INTRODUCTION

Oxide perovskite-type materials are widely applied in electroceramics because of their unique range of properties, including ferroelectricity and piezoelectricity (e.g. $BaTiO_3$, $Pb(Zr,Ti)O_3$), superconductivity and so-called colossal magnetoresistance (e.g. $LaMnO_3$) [1, 2]. These structures can also be found in optoelectronic applications (e.g. $LiNbO_3$), catalysis and in solar energy convertors (e.g. $SrTiO_3$) [3, 4]. Because of this, the development of new perovskite-type materials and/or the modification of existing ones remain a research focus.
The perovskite crystal structure ABO_3 is based on corner-linked octahedra BO_6 with a 12-coordinated larger cation A. This structure is stable only within the interval of the cations radii ratio, Goldschmidt's tolerance factor [5]. Only a small number of perovskite family members possess the ideal cubic structure of space group $Pm\bar{3}m$. When this is not the case, the ABO_3 stoichiometry is preserved, but the octahedra are distorted and/or tilted, forming orthorhombic, tetragonal or rhombic structures instead [6]. Some applications are based on these non-cubic structures (e.g., ferroelectrics, piezoelectrics or pyroelectrics) rather than on the actual perovskite structure itself.

In optics, rare-earth-doped $YAlO_3$ is one of the most applied materials, primarily as a laser host (doped with Er^{3+}, Tm^{3+}, Nd^{3+}), luminophore (doped with Tb^{3+} or Eu^{3+}) or scintillator (Ce^{3+} doped) [7, 8]. $YAlO_3$ possesses the orthorhombic crystal structure of space group *Pbnm* [9] and is routinely grown from a melt by the Czochralski technique. However, in a polycrystalline form, it tends to be meta-stable with another phase from the Y_2O_3–Al_2O_3 equilibrium being more stable, namely the $Y_3Al_5O_{12}$ garnet or $Y_4Al_2O_9$ monoclinic phase [10-14]. The perovskite structure can be stabilised when a larger cation is introduced (e.g. La^{3+}). Apart from the phase stabilisation, such a substitution moves the conduction band edge and, thereby, significantly influences the luminescence properties of the optical activators, which can be favourable for photoluminescence and scintillation applications.

In the case of Y/La substitution, the other end-member of the equilibrium ($LaAlO_3$) has the rhombic

crystal structure of space group $R\bar{3}c$ at room temperature. This structure is transformed into a cubic arrangement at high temperatures and/or high pressures [15, 16]. Like the $YAlO_3$ material, $LaAlO_3$ has excellent properties for optical applications [17]. However, the description of a $YAlO_3$–$LaAlO_3$ solid solution is inconsistent in the literature. All of the relevant papers agree that there is only limited mutual Y-La solubility in both phases. Some authors do not even attempt to determine this solubility, but rather describe the direct decomposition into secondary phases; when the solubility interval is defined, the data are inconsistent [18-20]. Such inconsistency is probably caused by the synthesis method used that can kinetically influence the stabilisation of ions in the A-position.

Due to the above-described possible dependence of the phase equilibrium on the crystalline form and method of preparation, we decided to map the phase stability of $(La,Y)AlO_3$ samples synthetised by Spark Plasma Sintering (SPS). To the best of our knowledge, the $YAlO_3$–$LaAlO_3$ phase equilibria have not been tested in SPS synthetised samples. Because of the downward shift of the conduction band edge, the activation of the perovskite by Ce^{3+} or Pr^{3+} is not suitable. The samples were doped by europium, the final stoichiometry being $La_{1-x-0.05}Y_xEu_{0.05}AlO_3$ (x = 0 – 0.65). In the prepared series, the phase composition as well as the photoluminescence and radioluminescence properties were tested.

EXPERIMENTAL

Sample preparation

Powder precursors with the composition of $La_{1-x-0.05}Y_xEu_{0.05}AlO_3$ (x = 0; 0.25; 0.45; 0.55; 0.65) were prepared by a reverse co-precipitation method – a process producing homogeneous precursors for the subsequent SPS of multi-component oxides [21]. The used starting compounds were lanthanum acetate hydrate (Strem Chemicals; 99.9 %), yttrium nitrate hexahydrate (Strem Chemicals; 99.9 %), aluminium nitrate nonahydrate (Lach-Ner; p.a.), europium acetate hydrate (Alfa Aesar; 99.999 % REO), ammonium hydrogen carbonate (Penta; p.a.) and triethanolamine (Lach-Ner; pure). The aluminium and yttrium nitrates were dissolved in water, the approximate concentration of the metal ions in each solution was 0.8 $mol \cdot L^{-1}$; their exact concentrations were determined by a gravimetric analysis. The stoichiometric amount of Eu_2O_3 was dissolved in diluted HNO_3 (1:1), the molar ratio of Eu_2O_3:HNO_3 being 1:7. The Al^{3+}, Y^{3+} and Eu^{3+} solutions were mixed together with dried $La(Ac)_3$ according to the required stoichiometry; the obtained solution was then diluted with water to achieve a total metal ion concentration of 0.16 $mol \cdot L^{-1}$. The precipitating solution was prepared by dissolving NH_4HCO_3 in distilled water and adding triethanolamine. The NH_4HCO_3 concentration was 1 $mol \cdot L^{-1}$ and the triethanolamine concentration was 5 $g \cdot L^{-1}$.

The metal ion solution was added dropwise into the precipitant solution while continuously being stirred. The solution volume ratio was 1:1. The obtained suspension was filtered using suction filtration and, afterwards, the filtration cake was washed twice with distilled water and once with ethanol. The precipitate was dried for 24 hours at 100 – 250 °C and then annealed for 30 minutes at 1000 °C.

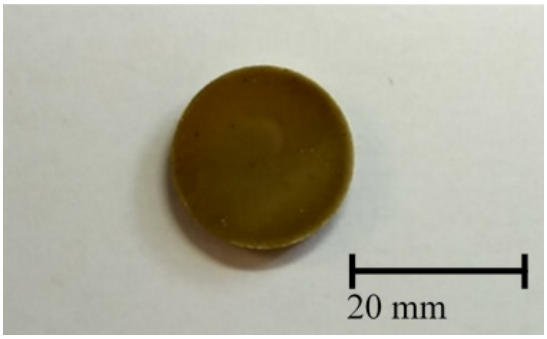

Figure 1. A polished as-sintered LYP sample.

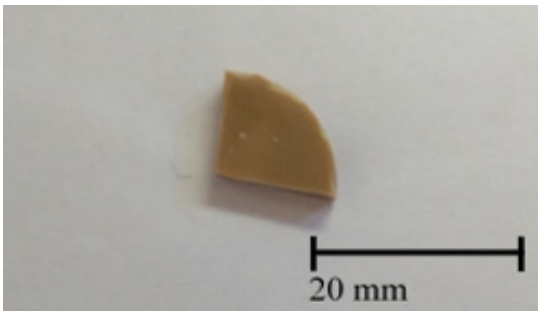

Figure 2. Sample after 1500 °C post-annealing.

The powder precursors were sintered using the SPS equipment (KCE-FCT HP D10, FCT Systeme GmbH). The samples were sintered in a graphite die. The sintering sequence consisted of several steps. A vacuum atmosphere (~ 5 Pa) was kept during the sintering. First, fast heating with a ramp of 100 $°C \cdot min^{-1}$ from the room temperature up to 1100 °C was applied with a pressure of 9.7 MPa. Then slow heating with a ramp of 10 $°C \cdot min^{-1}$ to 1350 °C with a pressure of 75 MPa followed. After a temperature of 1350 °C was achieved, a 20 min isotherm with a pressure of 75 MPa was applied. The sample was then cooled with a ramp of 50 $°C \cdot min^{-1}$ to 300 °C while continually releasing the pressure. The sintered samples were polished using a Galaxy Diamond Disc Red, a Galaxy Diamond Disc Blue and a Delta polishing cloth with a 9 μm diamond paste (all ATM GmbH). The samples had approximate dimensions of 20 mm (diameter) and 2.5 mm (height). The samples were broken into quarters and, finally, annealed at 1500 °C for 5 hours in oxygen.

Characterization methods

The phase composition of the precursors and final samples were determined by an X-ray powder diffraction (XRD) with an AXS D2 Phaser Bruker powder diffractometer with parafocusing Bragg–Brentano geometry and a CuKα X–ray source (α = 1.79021 A, U = 30 kV, I = 10 mA). The results were analysed and interpreted with the software HighScore Plus (PANanalytical, database PDF-4).

The bulk density of the samples was measured by the Archimedes method in distilled water.

The photoluminescence spectra were measured by a Fluorolog®-3 Extreme spectrometer (Horiba Jobin Yvon) using a photomultiplier with thermoelectric cooling and a Ce:InGaAs photocathode. Excitation was carried out with a 450 W xenon lamp in a continual mode. A monochromator with a double diffraction lattice for the excitation wavelength selection and one diffraction lattice for the emission wavelength selection was used. The spectra were collected in the reflection mode. For the spectra evaluation, all of the measured luminescence spectra were transformed to the base level and, after the subtraction of the background, normalised with the help of the reference sample was undertaken (a commercial Ce:YAG single crystal).

A 5000M spectrometer (Horiba Jobin Yvon) was used for the measurement of the photoluminescence decays. The spectra were collected using a photon-counting detector (TBX-04, IBH Scotland) with a monochromator with one diffraction lattice. The samples were excited by pulse nano-LEDs with the appropriate excitation wavelength. The radioluminescence spectra were measured by the same spectrometer (5000M, Horiba), but an X-ray Mo cathode (40 kV, 15 mA, Seifert GmbH) was used for the excitation. $Bi_4Ge_3O_{12}$ (BGO) phosphor was used as a standard for the comparison with the prepared samples.

RESULTS AND DISCUSSIONS

To investigate the influence of the La/Y ratio on the phase transformation between the $LaAlO_3$ and $YAlO_3$ perovskite-like structures and on their optical properties, we prepared a series of ceramic samples, in which La was gradually substituted by Y in $(La,Y)AlO_3$ up to 65 at. %. All the samples were doped with a concentration of 5 at. % Eu in the large cation crystal site. The sample composition and labelling are summarised in Table 1.

Table 1. List of the samples and their composition.

Sample name	LYP-00	LYP-25	LYP-45	LYP-55	LYP-65
x*	0	0.25	0.45	0.55	0.65

*x in $La_{1-x-0.05}Y_xEu_{0.05}AlO_3$

XRD phase analysis

First, the co-precipitated and annealed precursors were analysed using XRD (not presented). The desired perovskite-type phases $LaAlO_3$ or $YAlO_3$ were the major phases in all the cases, although their crystallinity was not well evolved. An Eu- and La-doped $Y_4Al_2O_9$ phase (known as YAM) was detected as a secondary phase, although only in concentrations bordering on the detection limit. In the case of the Y-free sample (LYP-00), La_2O_3 was found as the secondary phase in the precursor powder (at the detection limit, as well).

After the SPS processing, the samples were annealed in oxygen to secure the europium valence to be +III. The phase composition of those samples was also characterised by XRD (Figure 3). The gradual substitution of La^{3+} with Y^{3+} caused a change in the crystal structure. The sample without yttrium (LYP-00) and the sample with a lower concentration of Y^{3+} (LYP-25) were assigned to the $LaAlO_3$ rhombohedral structure ($R\bar{3}c$ space group). The lattice parameters were calculated using the Rietveld refinement (Table 2). In the case of the sample without yttrium (LYP-00), where larger La^{3+} was substituted only by smaller Eu^{3+} (ionic radii are 1.36 Å and 1.12 Å, respectively), the parameter *a* slightly decreased whereas *c* increased compared to the pure LaAlO3. Such an inconsistency could be caused by the anisotropic distortion of the rhombohedral structure connected with the octahedral tilting when a smaller cation is substituted in the A position [22]. However, in the LYP-25 sample, both lattice parameters decreased (the ionic radius of 12-coordinated yttrium is smaller that of lanthanum, 1.20 Å and 1.36 Å, respectively).

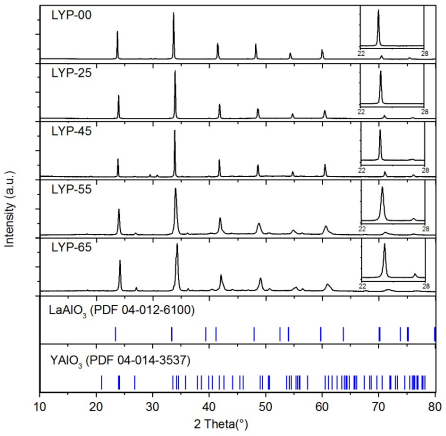

Figure 3. XRD of the SPS samples after post-annealing in an oxygen atmosphere; the inset illustrates the changes with the Y/La substitution described in the text.

At a higher yttrium content, the rhombohedral structure transformed into an orthorhombic phase (*Pbnm* space group) that characterises the $YAlO_3$ phase. However, the $LaAlO_3$-$YAlO_3$ phase transformation

did not exhibit a sharp boundary, moreover, it was not even clear if it is a mixture of pure rhombohedral and orthorhombic phases or of some Y-rich and La-rich distorted phases – both such concepts appear in literature [19, 20]. In any case, the samples LYP-45, LYP-55 and LYP-65 showed changes in their crystal structure that were demonstrated either by appearance of the XRD reflections of lower orthorhombic symmetry or by broadening the XRD reflections (where both orthorhombic and rhombohedral structures diffract). This phenomenon is illustrated in the inset of Figure 3 where, with the La-Y substitution, the diffraction peaks are broadened (the reflection of $LaAlO_3$ (012) is gradually mixed with the $YAlO_3$ (110) and (002)) and, consequently, a new diffraction appears at around 26.9° (the $YAlO_3$ (111) reflection). In the XRD measurement, the particular reflections are not well separated; it is, therefore, not clear whether we have a mixture of two distinct phases. In such a case, it would be a question if the structure analysis to derive the lattice parameters of the present phases is plausible. However, when we performed the Rietveld analysis with a presumption that $La_{0.95}Eu_{0.05}AlO_3$ and $Y_{0.95}Eu_{0.05}AlO_3$ are present, we obtained lattice parameters of these two supposed structures (see Table 2). The lattice parameters generally changed in the sense of the La/Y ratio; however, some inconsistencies can be observed due to the above-mentioned anisotropic deformability of the octahedra. Taking the changes into account, we can assume that a partial Y/La substitution takes place in both phases. Therefore, we could admit that the model is of a mixture of Y-rich and La-rich perovskite-type phases.

this trend probably caused by the non-systematic phase transformation. Due to the uncertain interpretation of the crystallographic data, the theoretical density cannot be precisely calculated. However, an approximate calculation showed that all the samples exhibit 92 – 98 % of the theoretical density (compared with the Eu-doped $LaAlO_3$ in the LYP-00 and LYP-25 cases, and with the Eu-doped $YAlO_3$ for the others).

Table 3. Results of the bulk density measurement.

Sample name	LYP-00	LYP-25	LYP-45	LYP-55	LYP-65
Bulk density	6.17	5.83	5.60	5.8	5.67

Photoluminescence and radioluminescence of samples

The photoluminescence (PL) spectra of the Eu^{3+} ions are definitely influenced by the gradual transformation between the $LaAlO_3$ and $YAlO_3$ structures due to the La/Y substitution. The photoluminescence excitation spectra are shown in Figure 4. The shift in the charge transfer excitation band probably originates from the changes in the O^{2-} energy levels, which define the top of the valence band, due to the La/Y substitution. The shift in the absorption edge to higher energies with the substitution by a smaller ion into the A-site is consistent with literature [23]. Weaker excitation bands appearing above 360 nm can be assigned to the f-f transitions of the Eu^{3+} ions [10, 24].

In the photoluminescence emission measurement (Figure 5), the samples were excited at different

Table 2. The lattice parameters of the Eu-doped perovskite-like phases – $La_{0.95}Eu_{0.05}AlO_3$ and $Y_{0.95}Eu_{0.05}AlO_3$.

Sample	$La_{0.95}Eu0_{.05}AlO_3$		$Y_{0.95}Eu_{0.05}AlO_3$		
	a (Å)	c (Å)	a (Å)	b (Å)	c (Å)
$LaAlO_3$*	5.3651	13.1113			
LYP-00	5.359(7)	13.144(9)			
LYP-25	5.333(1)	13.065(7)			
LYP-45	5.315(4)	13.021(8)	5.319(5)	7.50(3)	5.324(7)
LYP-55	5.318(0)	13.021(5)	5.317(1)	7.47(6)	5.266(1)
LYP-65	5.315(5)	12.937(0)	5.321(2)	7.46(8)	5.252(2)
$YAlO_3$**			5.1803	7.3706	5.3295

*reference card PDF 04-012-6100, ** reference card PDF 04-014-3537

Bulk density measurement

The bulk density of the samples is presented in Table 3. The bulk density follows the trend of the increasing yttrium substitution. First, yttrium has a lower mass and, second, $YAlO_3$ possesses lower density than $LaAlO_3$. However, there is a slight deviation from

wavelengths due to the shift in the charge transfer excitation band (LYP-00 was excited at 350 nm and the others at 270 nm). The emission spectra include transitions from the excited level $^5D_0$ of the Eu^{3+} ions to the basic multiplet ^7F_J (J = 1, 2, 3, 4, 5). With the substitution of La with Y, the Eu^{3+} local site symmetry

changes and, thus, the mutual intensity ratios among the different Eu^{3+} emission lines change. Moreover, other satellite emission lines appear in the samples with the $LaAlO_3$ phase or as an effect of the La substitution at the Y site in the $YAlO_3$ structure. This fact can be explained by the rather different sensitivity to the departures from the site inversion symmetry for the above mentioned Eu^{3+} transitions in both the $YAlO_3$ and $LaAlO_3$ structures [10, 24-26]. Not only does the relative intensity of the individual emission lines change, but the particular transitions are also split into a higher number of bands.

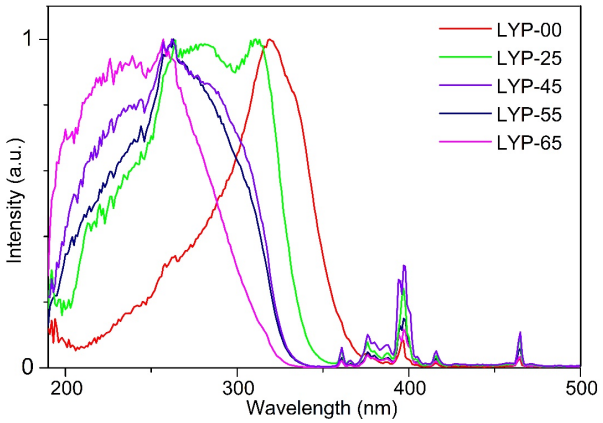

Figure 4. Normalised excitation photoluminescence spectra measured for the 615 nm emission.

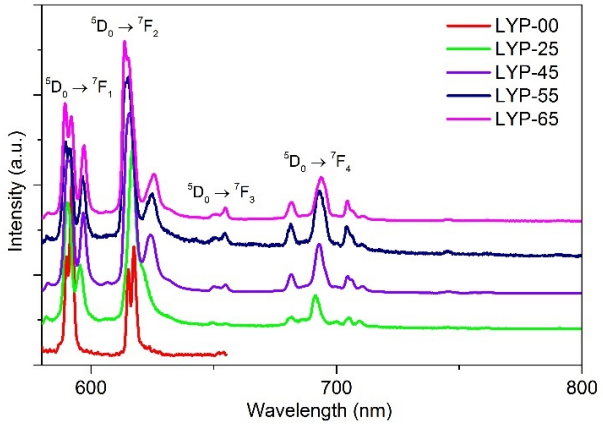

Figure 5. PL emission spectra of the samples (LYP-00 was excited at 350 nm and the others at 270 nm).

The time dependence of the intensity of the 615 nm PL emission line after the pulse excitation was also measured. In Figure 6, we can observe that the increasing content of Y^{3+} caused a slight acceleration in the PL decay. The data were fitted to obtain decay times of each component and its contribution to the overall intensity (Table 4 summarises these results). The departure from the single exponential course of the Eu^{3+} emission decay points to the presence

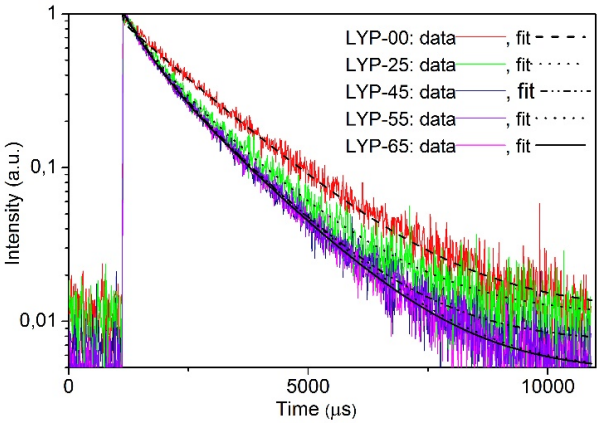

Figure 6. PL decay of the Eu^{3+} emission (λ_{exc} = 260 nm, λ_{em} = 615 nm).

of inequivalent Eu^{3+} sites. The two-exponential fit is a technical tool which quantitatively characterises such decays and changes in their time profile due to the change in the chemical composition of the host. In accordance with the fit results, the increasing Y^{3+} content caused the rise of the faster component τ_2 value (therefore slowing down), but also increase its contribution to the overall intensity which resulted in the overall acceleration of the PL decay. This is probably caused by the changes in the Eu^{3+} ions local symmetry in the A-site and eventual changes in the degree of covalence in the bonding of Eu^{3+} with the surrounding.

Table 4. Photoluminescence decay times obtained from the 2-exponential approximation ($I(t)$ = Ai · exp[-t/T_i] + background, i = 1,2).

Sample	τ_1 (μs)	I_1 (%)	τ_2 (μs)	I_2 (%)
LYP-00	1696	91.28	363	8.72
LYP-25	1571	78.97	582	21.03
LYP-45	1439	78.94	532	21.06
LYP-55	1475	80.12	498	19.88
LYP-65	1443	79.62	508	20.38

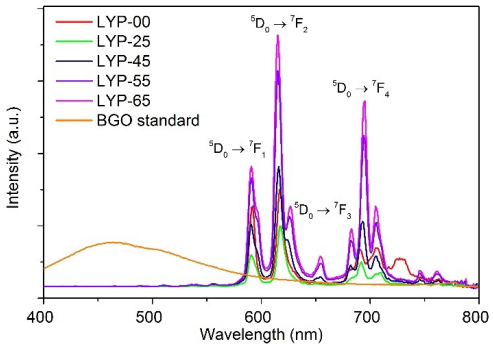

Figure 7. Normalised excitation photoluminescence spectra measured for the 615 nm emission.

The radioluminescence (RL) spectra had the same characteristics and trends as the photoluminescence spectra (Figure 7); the separation of the bands or energy shifts observed were similar to the PL emission spectra. Unlike the PL measurement, the RL spectra were carried out under the same excitation, therefore, the intensity of the emitted light can be compared among the samples. The intensities of the samples' emissions are compared to the BGO standard. The intensity of the emitted light integrated in a range of 500 – 800 nm increases with the Y^{3+} ion concentration (Figure 8). The origin of this effect remains unclear, but is most probably related to the changes in the effectivity of the energy transfer towards Eu^{3+} in the transfer stage of the scintillation mechanism.

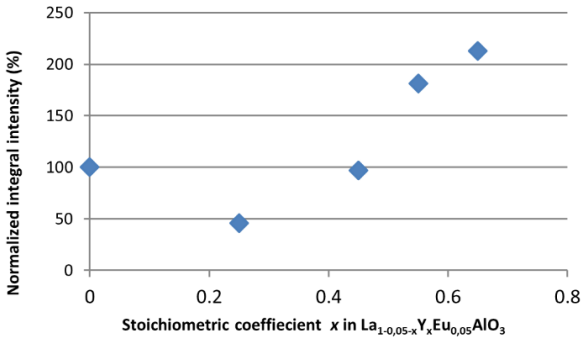

Figure 8. Composition dependence of the RL spectra integral intensity (in a range of 500 – 800 nm).

CONCLUSIONS

A series of polycrystalline samples with a composition of $La_{1-x-0.05}Y_xEu_{0.05}AlO_3$ (x = 0 – 0.65) was synthetised using Spark Plasma Sintering. The XRD analysis indicated that the samples are very likely a mixture of La-rich and Y-rich $(La,Y)_{0.95}Eu_{0.05}AlO_3$ phases rather than a stoichiometric mixture of Eu-doped $LaAlO_3$ or $YAlO_3$ phases. With La/Y substitution, the top of the valence band was shifted by the changes in the O^{2-} energy levels most probably arising from the different degree of covalency in the La-O bonds compared to the Y-O ones. This effect was demonstrated mainly in the excitation spectra where the charge transfer excitation was dominant in the UV spectral region. Both photoluminescence and radioluminescence emission spectra were composed of the typical 4f-4f energy transitions of Eu^{3+} ions. The Eu^{3+} local site symmetry and bonding to the surrounding changes with the La/Y substitution and is reflected in the changing intensity ratios among the Eu^{3+} emission lines and appearance of satellite ones. Furthermore, the photoluminescence kinetics accelerated with the increasing La content. The integral intensity of the radioluminescence spectra was enhanced with the increasing La substitution at the Y sites.

Acknowledgment

This work was supported by the Ministry of the Interior of the Czech Republic Grant no: VI20192022152.

REFERENCES

1. Ishihara T. (2017). Inorganic perovskite oxides. In *Springer Handbook of Electronic and Photonic Materials* (pp. 1-1). Springer, Cham. doi: 10.1007/978-3-319-48933-9_59
2. Moure C., Peña O. (2015): Recent advances in perovskites: Processing and properties. *Progress in Solid State Chemistry, 43*(*4*), 123-148.doi: 10.1016/j.progsolidstchem.2015.09.001
3. Hwang J., Rao R. R., Giordano L., Katayama Y., Yu Y., Shao-Horn, Y. (2017): Perovskites in catalysis and electrocatalysis. *Science, 358*(6364), 751-756. doi: 10.1126/science.aam7092
4. Arizmendi L. (2004): Photonic applications of lithium niobate crystals. *physica status solidi (a)*, *201(2)*, 253-283. doi: 10.1002/pssa.200303911
5. Johnsson M., Lemmens P. (2008): Perovskites and thin films—crystallography and chemistry. J*ournal of physics: condensed matter, 20*(26), 264001.doi: 10.1088/0953-8984/20/26/264001
6. Woodward P. M. (1997): Octahedral tilting in perovskites. I. Geometrical considerations. *Acta Crystallographica Section B: Structural Science, 53*(1), 32-43. doi: 10.1107/s0108768196010713
7. Baccaro S., Blaŝek K., De Notaristefani F., Maly P., Mares J. A., Pani R.,et al. (1995): Scintillation properties of YAP: Ce. *Nuclear Instruments and Methods in Physics Research Section A: Accelerators, Spectrometers, Detectors and Associated Equipment, 361*(1-2), 209-215. doi: 10.1016/0168-9002(95)00016-x
8. Gansheng L., Zhenzhu S., Xibin G., Jinhua W., Ying C., Jinfeng C. (1990): Growth and characterization of high-quality Nd^{3+}: YAP laser crystals. *Journal of Crystal Growth, 106*(4), 524-530.doi: 10.1016/0022-0248(90)90025-G
9. Senyshyn A., Vasylechko L. (2013): Low Temperature Crystal Structure Behaviour of Complex Yttrium Aluminium Oxides $YAlO_3$ and $Y_3Al_5O_{12}$. *Acta Physica Polonica A, 124*(2), 329-335. doi:10.12693/APhysPolA.124.329
10. Gao H., Wang Y.H. (2007): Photoluminescence of Eu^{3+} Activated $YAlO_3$ under UV-VUV Excitation. *Materials Research Bulletin, 42*(5), 21-927. doi: 10.1016/j.materresbull.2006.08.010
11. Inoue T., Morimoto T. et al. (2015): Experimental Observations on the Crystalline Structures of $YAlO_3$ Single Crystal at High Temperatures. *Applied Physics a-Materials Science & Processing, 119*(4), 1423-1429. doi:10.1007/s00339-015-9115-2
12. Jin Z.P., Chen Q. (1995): An Assessment of the $AlO_{1.5}$-$YO_{1.5}$ System. *Calphad-Computer Coupling of Phase Diagrams and Thermochemistry, 19*(1), 69-79. doi:10.1016/0364-5916(95)00008-3
13. Gieszczyk W., Bilski P., et al. (2019): Luminescent Properties of Undoped and Ce^{3+} Doped Crystals in Y_2O_3-Lu_2O_3-Al_2O_3 Triple Oxide System Grown by Micro pulling-down Method. *Optical Materials, 89*, 408-413. doi:10.1016/j.optmat.2019.01.023

14. Harada M., Goto M. (2006): Synthesis of Y-Al-O Compounds by a Polymer Complex Method. J*ournal of Alloys and Compounds, 408*, 1193-1195. doi:10.1016/j.jallcom.2004.12.118
15. Hayward S.A., Morrison F.D., et al. (2005): Transformation Processes in $LaAlO_3$: Neutron Diffraction, Dielectric, Thermal, Optical and Raman Studies. *Physical Review B, 72*(5),17. doi:10.1103/PhysRevB.72.054110
16. Zhao J., Ross N.L., et al. (2004): Polyhedral Control of the Rhombohedral to Cubic Phase Transition in $LaAlO_3$ Perovskite. *Journal of Physics-Condensed Matter, 16*(47), 8763-8773. doi:10.1088/0953-8984/16/47/026
17. Pejchal J., Barta J., et al. (2019): Luminescence and Scintillation Properties of Rare-earth-doped $LaAlO_3$ Single Crystals. *Radiation Measurements, 121*, 26-31. doi:10.1016/j.radmeas.2018.11.010
18. Fabrichnaya O., Savinykh G., et al. (2013): Phase Relations in the ZrO_2-La_2O_3-Y_2O_3-Al_2O_3 System: Experimental Studies and Phase Modelling. *Journal of the European Ceramic Society, 33*(1), 37-49. doi:10.1016/j.jeurceramsoc.2012.08.020
19. Kyomen T., Itoh M. (2002): Calorimetric and Structural Studies of $La_{1-x}Y_xAlO_3$ and $Y_{1-x}Lu_xAlO_3$ Crystals. *Journal of Thermal Analysis and Calorimetry, 69*(3), 813-819. doi:10.1023/a:1020647704262
20. Vasylechko L., Senyshyn A., et al. (2009): Perovskite-type aluminates and gallates. *Handbook on the physics and chemistry of rare earths, 39*, 113-295.doi:10.1016/s0168-1273(08)00002-0
21. Thor T., Rubesova K., et al. (2021): Dense Ceramics of Lanthanide-doped Lu_2O_3 Prepared by Spark Plasma Sintering. *Journal of the European Ceramic Society, 41*(1), 741-751. doi:10.1016/j.jeurceramsoc.2020.08.028
22. Howard C.J., Kennedy B.J., et al. (2000): Neutron Powder Diffraction Study of Rhombohedral Rare-earth Aluminates and the Rhombohedral to Cubic Phase Transition. *Journal of Physics-Condensed Matter, 12*(4), 349-365. doi:10.1088/0953-8984/12/4/301
23. Hoefdraad, H.E. (1975): Charge-transfer Absorption-band of Eu^{3+} in Oxides. *Journal of Solid State Chemistry, 15*(2),175-177. doi:10.1016/0022-4596(75)90242-x
24. Lee, S.H., P. Du, et al. (2017): Ultraviolet Radiation Excited Strong Red-emitting $LaAlO_3$:Eu^{3+} Nanophosphors: Synthesis and Luminescent Properties. *Ceramics International, 43*(5), 4599-4605. doi:10.1016/j.ceramint.2016.12.123
25. Singh, V., S. Watanabe, et al. (2011): Characterization, Photoluminescence, Thermally Stimulated Luminescence and Electron Spin Resonance Studies of Eu^{3+} Doped $LaAlO_3$ Phosphor. *Solid State Sciences, 13*(1), 66-71. doi:10.1016/j.solidstatesciences.2010.10.010
26. Moon, B.K., I.M. Kwon, et al. (2007): Synthesis and Photoluminescence of Eu^{3+} in $Y_{1-x}Gd_xAlO_3$ Nanophosphors. *Physica Scripta, T129,* 284-287. doi:10.1088/0031-8949/2007/t129/063